A Comparison of Industrial-Scale Radiometer Heat Flux Measurements Between Pulverized-Coal and Coal/Biomass Co-Firing Combustion

(article starts on next page)

Teri S. Draper[1]
Department of Chemical Engineering,
University of Utah,
50 South Central Campus Drive,
Room 3290 (MEB),
Salt Lake City, UT 84112
e-mail: teri.draper@utah.edu

Adrian Gunnarsson
Department of Space, Earth and Environment,
Chalmers University of Technology,
Gothenburg SE-412 96, Sweden
e-mail: adriang@chalmers.se

Andrew Fry
Department of Chemical Engineering,
Brigham Young University,
Provo, UT 84602
e-mail: afry@byu.edu

Klas Andersson
Department of Space, Earth and Environment,
Chalmers University of Technology,
Gothenburg SE-412 96, Sweden
e-mail: klon@chalmers.se

Terry Ring
Department of Chemical Engineering,
University of Utah,
Salt Lake City, UT 84112
e-mail: ring@chemeng.utah.edu

Eric Eddings
Department of Chemical Engineering,
University of Utah,
Salt Lake City, UT 84112
e-mail: eric.eddings@chemeng.utah.edu

A Comparison of Industrial-Scale Radiometer Heat Flux Measurements Between Pulverized-Coal and Coal/ Biomass Co-Firing Combustion

This work evaluates and compares radiative heat transfer measurements conducted at the $471-\mathrm{MW}_E$ Hunter Power Plant Unit 3 utility boiler in Utah, United States, during standard operation with coal and also co-firing with biomass. The coal used was a Utah-sourced bituminous coal, which was mixed with torrefied wood (15% by weight) for the co-firing test. Radiation from the flame was measured using radiometers of three different designs. Data were gathered at three elevations along the boiler wall. Overall, the measured heat fluxes and corresponding temporal variations decreased with increasing boiler elevation. While the variation in the replicates of the heat flux data is notable, a statistical analysis indicates that the heat flux profile at the elevations investigated is not significantly affected by the change in fuel. [DOI: 10.1115/1.4056537]

1 Introduction

Biomass is an abundant resource that can be used to produce renewable energy. In 2020, it provided roughly 5% of the energy consumed in the United States [1]. There is ever-strengthening concern to reduce net CO_2 emissions in the energy industry. Dreizler et al. [2] discuss the need to utilize carbon-neutral, renewable energy sources in order to implement climate neutrality into the world wide energy industry. Advancements in the implementation of biomass combustion are necessary to achieve this goal. Currently, the cost (both monetarily and in terms of CO_2 expenditure) to harvest and transport biomass is higher—often significantly—than when using fossil fuels [3,4]. However, there is also motivation to manage the forestlands in the United States. Co-firing biomass in power plants near these forests could prove symbiotically beneficial to both wildfire management and lowering CO_2 emissions [5].

While there are myriad ways to utilize biomass in energy production, biomass co-firing is commonly seen as the optimal solution [6]. It is relatively easy to deploy, requires few furnace modifications, can reduce other pollutant emissions when strategically implemented, and can readily switch between running purely on fossil fuels when biomass fuel is not available [7].

For biomass co-firing to be feasible, any changes to the heat transfer in the boiler must be minimal. Many co-firing tests have been run at full-scale utility boilers to evaluate this impact [7–11]. However, these tests typically rely solely on the operational data routinely collected at the plants, which can be limited in scope and do not include incident heat flux measurements.

More commonly, data to analyze the potential effects of biomass co-firing are taken at smaller scales [12–20], which can then be extrapolated to the industrial-scale through modeling. Pilot and particularly laboratory scales allow for much more control, repeatability, accessibility, and flexibility in choice of measurement technique than at the scale of interest. However, the relative ease of experimenting at smaller scales must be tempered with caution in extrapolating the conclusions to the industrial scale. Bäckström et al. [21] reported unexpected differences in heat transfer trends in a 400 kW test furnace when firing two very similar coals. The paper emphasized the need to measure radiative heat transfer from flames "under conditions representing the applications of interest." The computer simulation of biomass co-firing in industrial boilers is of great import because of the large diversity in biomass sources and the extreme cost and difficulty of performing experiments at this scale. Milićević et al. [22] numerically examine the effect of co-firing pulverized-coal with three types of agricultural residues at three different boiler loads. Qin et al. [23] utilize boiler operational data, two-color pyrometry, and NO_x measurements to create an online deep learning model that can predict NO_x emissions in oxy-biomass combustion. Providing experimental data at the scale of interest enables better verification and validation of these complex models.

Optical methods are often appropriate for industrial applications due to their non-invasive nature. Radiometers are particularly apt

---

[1]Corresponding author.
Manuscript received September 14, 2022; final manuscript received November 19, 2022; published online January 11, 2023. Assoc. Editor: George S. Dulikravich.

Fig. 1 Images of University of Utah narrow-angle radiometer setup at each boiler elevation examined

due to their relatively simple setup and operation, along with the ability to function well in harsh environments. As such, the use of radiometers is extremely common in measuring radiative heat transfer in many combustion situations [21,24–32]. Presently, there is a limited number of studies presenting radiative heat flux data at industrial-scale. As radiation is the dominant heat transfer mechanism in industrial boilers [33], experimental heat flux measurements are very important to facilitate the accurate modeling of these boilers. Costa et al. [34] took incident wall heat flux measurements with a radiometer as well as local gas species concentrations and temperatures in a 300 MW_E utility boiler. Li et al. [35] measured gas species, temperatures, char burnout, and wall heat flux in a 200 MW_E utility boiler. They utilized an optical pyrometer to present the heat flux profile of the boiler in four elevations at three different loads. Butler and Webb [36] reported local temperature and wall heat flux measurements in an 80 MW_E coal-fired boiler. The heat flux measurements were taken with an ellipsoidal radiometer (ER) at six boiler elevations. These measurements were repeated in a subsequent paper with the addition of particle temperature measurements and results were compared when firing two different coals [37]. With the exception of Costa et al. [34], these papers do not present any replicates of the heat flux measurements. None of the papers indicate the level of temporal variability seen during each measurement. Neither do any present heat flux data with taken with multiple instruments. One of Butler and Webb papers examines [37] two types of coal, but none of the above papers examine the effect of biomass co-firing on radiative heat flux.

The objective of this work is to present radiative heat transfer data in a 471 MW_E utility boiler. Furthermore, a comparison of heat transfer profiles between standard pulverized-coal operation and co-firing a coal/biomass blend is presented to identify the effects of co-firing on the system. These data, while somewhat preliminary, are valuable as they provide the heat flux profile of the boiler at both conditions, provide insight regarding the feasibility of biomass co-firing, and yield insights on taking additional data in such challenging conditions in the future.

This work was done in collaboration with multiple teams of experimentalists who performed the following:

(1) Incident wall radiation measurements (University of Utah, Chalmers University).
(2) Deposit and entrained aerosol ash sample measurements (Brigham Young University, University of Utah).
(3) Nitric oxide (NO) measurements (Chalmers University).
(4) Various plant impact measurements (PacifiCorp, Brigham Young University).

Item (1) is the sole subject of this study. Li et al. [38] have published their findings from Item (2). They concluded that fly ash and aerosol size distributions and compositions are broadly unchanged when co-firing. They also saw a reduction in total deposition amount when co-firing with only slight differences in deposit composition. Allgurén et al. [39] have published their findings from Item (3), which show that co-firing reduced NO formation

beyond what could be expected solely from the reduction in fuel nitrogen. Not all measurements taken during Item (4) have yet been published.

2 Experimental Description

2.1 Hunter Power Plant. The experimental work discussed in this paper was conducted at the Rocky Mountain Power Hunter Power Plant, which is located in central Utah. The experimental work presented here was conducted on Unit 3, which provides the electrical grid with 471-MW_E through the combustion of pulverized-coal. The total inner height of the boiler is roughly 51
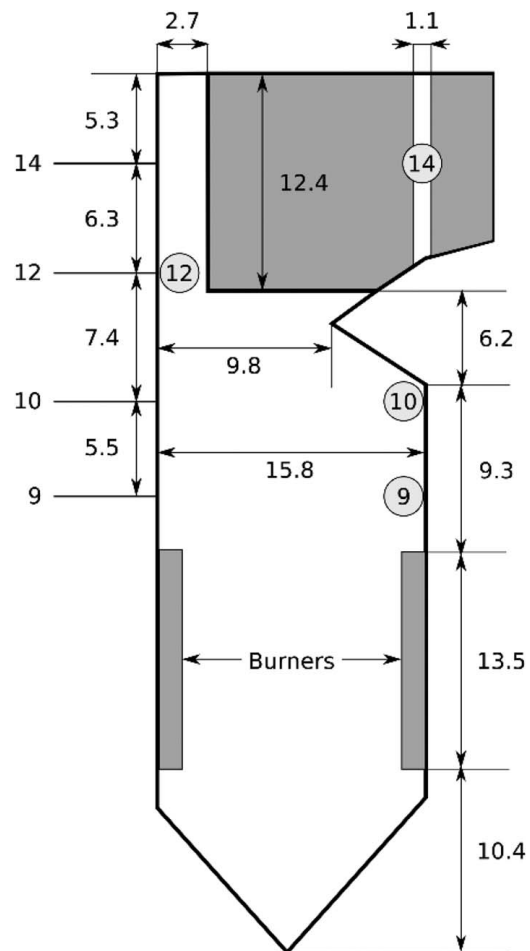

Fig. 2 Simplified schematic of the Hunter Power Plant Unit 3 boiler. Locations of measurement ports on Floors 9, 10, 12, and 14 are labeled. Dimensions are given in meters. The gray region near Floor 14 represents heat exchange tube banks.

Table 1 Ultimate analysis (% mass, as rec'd) of the fuels used in campaign

|	Coal	Biomass	Blend
C	63.3	47.7	61.0
H	4.43	5.20	4.55
N	1.23	0.23	1.08
S	0.48	0.02	0.41
O	10.4	35.6	14.2
Ash	11.6	0.85	10.0
Moisture	8.5	10.4	8.74
Higher heating value (MJ/kg)	25.8	19.1	24.8

Fig. 3 Exploded view schematic of the narrow-angle radiometer used by the University of Utah (UofU NAR). The probe includes the following components: 1, 3, 5—Swagelok fittings, 2—thermopile, 6—tubing, 7—output cable, 8—view tube, and 9—O-ring. [40], Reprinted with permission from Elsevier © 2018.

m with a maximum cross section of 15.3×15.8 m. Measurements presented in this paper were conducted through ports in the furnace wall located at Floors 10, 12, and 14 (Figs. 1 and 2). These ports are located above the burners. During the experimental work, the unit was operated at 90% load with normal burner and staging operating conditions.

2.2 Fuel Conditions. In the experimental test campaign, two different fuel conditions were studied. The baseline case utilized the Utah-sourced bituminous coal primarily used to fuel the unit. The co-firing case utilized the same coal (85% by weight) and a torrefied, pelletized, woody biomass (15% by weight) sourced from local Utah forests and produced by Amaron Energy in Salt Lake City. The biomass was collected from the Wasatch-Cache National Forest roughly 150 miles from the Hunter Power Plant. This biomass is very similar in composition to that of Manti-La Sal National Forest, the border of which is only 20 miles from the Hunter Power Plant. Minimizing the distance from the biomass source to the plant is important to make biomass utilization feasible. The ultimate analysis for the coal, the torrefied biomass, and a calculated coal/biomass co-firing blend analysis are shown in Table 1. For the co-firing case, the coal and biomass pellets were milled together at the plant and then directly fed to the burners. Each fuel condition was tested for a 24 h period, which required roughly 720 tons of biomass during the co-firing case. It took approximately 8 h of operation with the biomass blend before the biomass percentage in the fuel flow stabilized.

2.3 Measurement Devices. Researchers from several universities collaborated to take data that included wall radiation, gas composition, deposit, and aerosol ash sampling, as well as the standard operational (PI) data measured by the plant. However, the work presented in this paper focuses solely on the radiative heat transfer data, which were obtained using the following three instruments:

- UofU NAR: The University of Utah (UofU) used a narrow-angle radiometer (NAR) to measure the narrow-angle radiative intensity.
- CTH NAR: Chalmers University of Technology (CTH) used a separate NAR to measure the narrow-angle radiative intensity.
- CTH ER: Chalmers University of Technology used an ER to measure the wide-angle radiative heat flux.

Radiation data from all three instruments were taken at three elevations in the boiler (Floors 10, 12, and 14).

2.3.1 Narrow-Angle Radiometer—The University of Utah. The narrow-angle radiometer used by the University of Utah (UofU NAR) was initially developed for use in a high pressure oxy-fuel combustor, the construction of which is detailed in Dobó [40]. Briefly, a thermopile detector is installed at the end of small diameter (ID of 3.5 mm) view tube 305 mm in length (see Fig. 3). The thermopile absorbs incoming radiation onto a small detector (0.49 mm^2) which then outputs a corresponding voltage. The inside of the view tube is coated with pulverized-coal to eliminate scattering onto the detector from rays not in the line-of-sight.
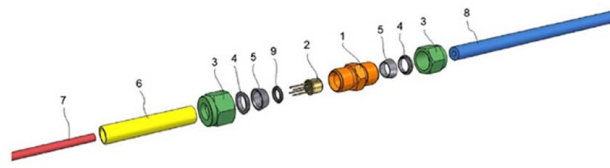
This, coupled with the relatively long view tube, results in a narrow field of view (FOV) (6.70×10^{-5} sr). Thus, this probe measures radiative intensity. A thermistor located on the non-irradiated side of the thermopile provides an ambient temperature measurement, which is necessary to account for any changes in ambient conditions between calibration and operation. The radiometer was placed in a water-cooled water jacket during data collection, with a nitrogen purge flowing over it to prevent any interfering media in the line-of-sight path. During the data collection, the radiometer was centered in each measurement port facing directly into the boiler.

2.3.2 Narrow-Angle Radiometer—Chalmers University of Technology. The narrow-angle radiometer instrument used by Chalmers University (CTH NAR) has been used in several previous studies to measure the radiative heat transfer in various flame conditions [21,26–28]. To ensure a narrow view angle, the probe has a total length of 2.3 m with an inner tube diameter of 1 cm. A thermopile detector is installed at the back end of the probe and a lens is used to concentrate the light to the detector (Fig. 4). With its narrow field of view (1.23×10^{-5} sr), the instrument can be considered to measure exclusively the radiative intensity in its line-of-sight. The inner tip of the probe is threaded to remove reflections in the inner tube wall. A small flow of nitrogen is used to prevent any gases or particles entering the probe in order to prevent signal distortion or probe damage. To prevent the probe from bending in the high temperature environment, it was constructed of titanium and is water-cooled during operation.

To maintain a constant sensor temperature, a separate cooling system is typically applied to the probe and the sensor housing. However, in the rugged conditions of the power plant, this refrigeration system was not feasible to use. A high flowrate of cooling water was used in its place to keep the sensor temperature as cool and stable as possible. The measured voltage signal from the thermopile corresponds to the radiative intensity incident on the detector. This signal is dependent on the temperature of the sensor as well. Neither the cooling water nor sensor temperature was directly measured, so—given the high temperature at the measurement locations (roughly 55 °C)—the sensor temperature was assumed to be 45 °C during these experiments. The narrow line-of-sight of the probe allowed for separate measurements with the probe directed in various directions within the boiler (e.g., boiler walls, center of the flame, etc.). At each of three elevations, measurements in
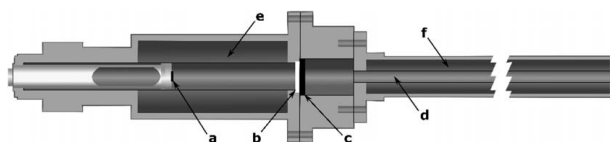

Fig. 4 Schematic of the narrow-angle radiometer used by Chalmers University (CTH NAR) to measure the radiative intensity from the flame. The probe includes the following components: (a) thermopile sensor, (b) focusing lens, (c) shutter, (d) collimating tube, (e) water-cooled sensor housing, and (f) water-cooled probe housing.
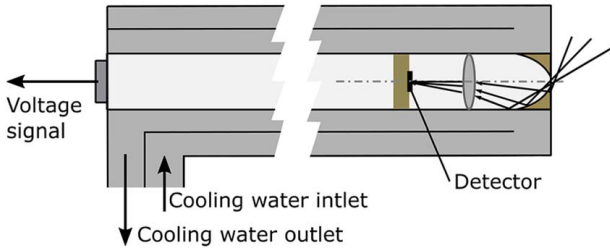
Fig. 5 Schematic of the ellipsoidal radiometer used by Chalmers University (CTH ER) for measuring the total radiative heat flux from the flame

multiple directions were conducted in order to provide comparisons with both the UofU-NAR data (pointed toward the center of the boiler) and the ellipsoidal radiometer data (using different view angles to combine measurements in various directions to approximate total heat flux).

2.3.3 Ellipsoidal Radiometer—Chalmers University of Technology. The incident total radiative heat flux to the furnace wall was measured using an ellipsoidal radiometer from Chalmers University (CTH ER). Radiation enters through a small orifice at the tip of a water-cooled probe into a highly-reflective, gold-plated cavity. The radiation is then focused via a lens onto a thermopile detector (Fig. 5). In contrast with the NAR probes, the view angle for this detector is close to hemispherical and the detector's voltage signal corresponds to all incident radiation reaching the measurement position, thus approaching the total radiative heat flux. During the measurements, the probe was centered in each measurement port with the probe tip directed straight into the center of the boiler.

3 Measurement Calibration

3.1 Narrow-Angle Radiometer Calibration. Each of the two narrow-angle radiometers used has a different calibration curve, but the form of the physics-based calibration equation—hereafter referred to as the instrument model—is the same for both. A brief summary of the instrument model will be presented and further details can be found by referring to Spinti et al. [41]. First, an energy power balance on the radiometer detector is performed

$$\Phi_d = \Phi_s + \Phi_a + \Phi_w - \Phi_e \qquad (1)$$

where the left-hand-side is the net radiant power at the detector (d), and the terms in the right-hand-side correspond to the different radiative contributions from the source (s), detector housing (a), radiometer tube wall (w), and the radiation emitted from the detector itself (e).

The net radiant power at the detector is assumed to be directly proportional to its output voltage (V), where $\Re$ is the electrical responsivity (mV/kW) of the detector

$$\Phi_d = \frac{V}{\Re} \qquad (2)$$

The radiative contribution from the source (Φ_s) is a function of the radiative intensity from the source (I_s) and various constant parameters (e.g., the magnification from the detector lens, the area of detector, the view angle from the source to the detector, etc.). The contribution from the detector housing is a function of constant parameters and the housing temperature to the fourth power. For the UofU NAR, it was assumed that the detector housing temperature was the same as the measured ambient temperature of the backside of the detector, T_a. For the CTH NAR, the housing was assumed to be at the cooling water temperature, which was assumed to be 45 °C. The same assumptions were employed for the temperature of the view tube walls for each NAR. The emitted power from the detector (Φ_d) is a function of constant parameters and the detector temperature (T_d), which is not directly measured but can be

Table 2 Fit coefficients and associated 95% confidence intervals used in narrow-angle radiometer instrument models

Parameter	UofU NAR		CTH NAR	
	Fit value	95% CI	Fit value	95% CI
K_1	24.3	0.870	64.0	18.0
K_2	1.60×10^{-8}	9.53×10^{-10}	4.14×10^{-9}	1.97×10^{-9}
K_3	1.58×10^{-8}	9.32×10^{-10}	2.57×10^{-9}	1.70×10^{-9}
K_4	24.9	1.12	175	54.5

calculated from the measured ambient temperature (T_a) on the backside of the detector. This calculation is done by adding the output voltage multiplied by a proportionality constant (the ratio of the thermal resistance, R_t (K/kW) and the electrical responsivity of the detector) to the ambient temperature

$$T_d = T_a + \frac{R_t}{\Re} V \qquad (3)$$

Combining these functions and grouping unknown constant parameters together yields an instrument model relating the source intensity to the measured thermopile voltage and ambient temperature:

$$I_s = K_1 V - K_2 T_a^4 + K_3 (T_a + K_4 V)^4 \qquad (4)$$

Blackbody generators were used to provide known radiative intensity values to calibrate both NARs at different ambient temperatures. The UofU NAR was calibrated with blackbody temperatures from 600 °C to 1500 °C in 100 °C increments and at three ambient temperatures (18, 32, and 46 °C). The CTH NAR was calibrated with a separate blackbody unit between 400 °C and 1500 °C in 100 °C increments at two ambient temperatures (20 and 45 °C). The MATLAB nonlinear "fit" function was used with each radiometer's calibration data to find the best-fit values for the coefficients K_1–K_4 and the associated 95% confidence intervals, which are summarized in Table 2. As shown in Table 2, each of the four calibration parameters are on a similar scale between the two radiometers. The differences in the coefficient magnitudes between the two radiometers are due to the differences in the radiometer design (e.g., different thermopiles, different dimensions, different view angles, etc.).

3.2 Ellipsoidal Radiometer Calibration. Due to the hemispherical view angle of the CTH ellipsoidal radiometer, a blackbody with its narrow radiating cavity was not an appropriate choice as a calibration source. Thus, the CTH ER was sent to an external laboratory where it was calibrated with an integrating sphere. Calibration data points were taken with the integrating sphere at temperatures between 600 °C and 1050 °C in 50 °C increments. The relationship between the output voltage and the source's heat flux was linear. The following empirical calibration equation was used rather than an equation with a form derived from an energy balance

$$E_s = 44.04 V + 0.0602 \qquad (5)$$

3.3 Total Heat Flux Model. Using the CTH NAR, the narrow-angle intensity was measured in several directions at each boiler elevation. By rough estimations of the probe angles during these measurements and the boiler dimensions (Fig. 2), the total radiative heat flux was estimated by adding the contribution from each measured direction multiplied by its corresponding view factor. Considering the detector area to be infinitesimal in

Table 3 Calculated view factors of interior boiler surfaces

View factor	Floor 10	Floor 12	Floor 14
F_L	0.31	0.26	0.46
F_R	0.11	0.11	0.46
F_O	0.24	0.17	0.01
F_{SH}	0.00	0.35	0.00
F_T	0.19	0.04	0.03
F_B	0.15	0.07	0.04

comparison to the boiler, the view factors were found from the expression

$$F_{ij} = \int_{A_j} \frac{\cos \theta_i}{\pi} \, d\Omega_j \qquad (6)$$

where θ_i is the polar angle from the probe tip to one end of a wall (e.g., the top of the right wall) and $d\Omega_j$ is the solid angle from the wall toward the probe tip. Considering the area of a narrow wall section, described by a small azimuthal angle ($\Delta\phi$), being projected to the surface of a unit hemisphere, a view factor from the small probe tip to a furnace wall can be expressed as the sum of the view factors for all narrow wall sections

$$F_{ij} = \sum_{\phi} \frac{\sin(\theta_i)\Delta\phi}{2\pi} \qquad (7)$$

Port 10 was positioned below the nose of the furnace (right wall in Fig. 2), while Port 12 was positioned at the opposite wall (left wall in Fig. 2) at the height of the lower end of the superheater (SH). Port 14 was positioned between the superheater and the convection path tubes (wall facing the reader in Fig. 2). The roughly approximated view factors from the left wall (L), right wall (R), directly opposite (O) wall, SH, as well as the top (T) and bottom (B) of the furnace are presented in Table 3 for Floors 10, 12, and

14. These view factors are used in conjunction with the CTH NAR measurements in the associated direction to approximate a total incident heat flux at each measurement elevation.

4 Results and Discussion

4.1 Radiation Measurements. Narrow-angle radiative intensities were measured using two different NAR probes in ports at three different floors at the Hunter Power Plant Unit 3. The total radiative heat flux was measured at the same positions using an ellipsoidal radiometer. To compare both measurement techniques more easily, the radiative intensities were recalculated into radiative heat fluxes by assuming the measured incident intensities to be diffuse (assuming uniform intensity across all directions). With this assumption, the conversion from measured flame intensity (I_s, (kW/m²/sr)) to total heat flux (E_s, (kW/m²)) is quite simple

$$E_s = \pi I_s \qquad (8)$$

As shown in subsequent results, this assumption of diffuse emission is not perfectly valid, as we measure smaller intensities at the periphery versus the center of the flame. However, the comparison is still deemed useful. Thus, the results from all three probes are presented in units of heat flux.

The measured radiative heat fluxes are presented in Fig. 6 for both fuel conditions at Floors 10, 12, and 14 as a function of time. The UofU measurements lasted roughly 30 min per replicate with a sampling frequency of roughly one measurement per second. The width of each data point's rectangular marker corresponds to the time duration of the measurement. The measurement times for the two CTH probes were much shorter (typically 30–60 s), and the width of the corresponding data markers is not correlated to the measurement duration. Both CTH probes utilized a sampling frequency of approximately 10 Hz. The UofU NAR probe was used twice for each case and floor and was directed toward the center of the furnace. The data presented in Fig. 6 from the CTH NAR were
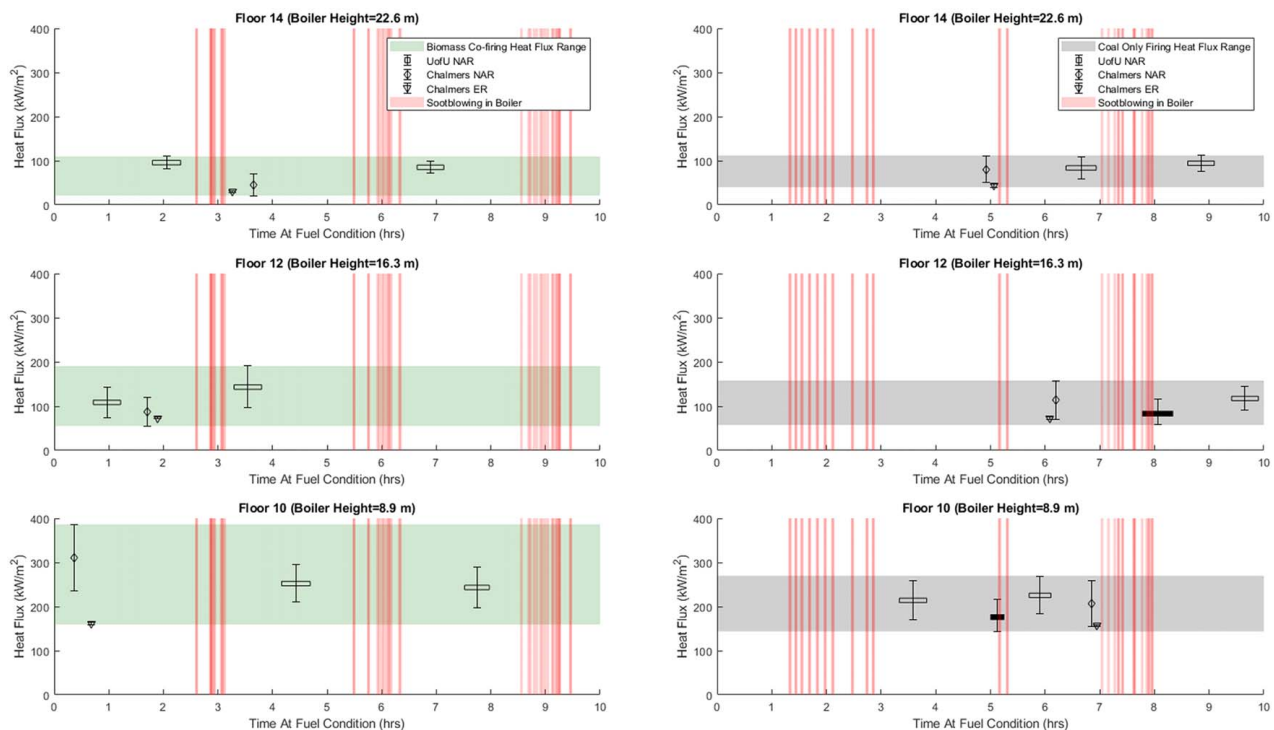

Fig. 6 Measured radiative heat fluxes for the three radiometers used during co-firing and coal fuel conditions at Floors 10, 12, and 14 as a function of time. "Boiler Height" refers to height in meters above the burners. Horizontal shaded regions indicate total variation in heat flux results at a given floor and fuel condition. Vertical shaded regions indicate times of soot blowing in the boiler.

also conducted with the probe directed toward the center of the furnace, although measurements with this probe pointed in additional directions are presented later. The average heat flux for each instrument is plotted with error bars representing two standard deviations of the temporal variation in the signal at each replicate. The horizontal regions on the plots indicate the total variation in heat flux measurements between the three instruments at a given fuel condition and height in order to aid comparison between fuels. During the experimental campaign, soot blowing was periodically conducted from the blowers located along the walls of the boiler in to clear deposit accumulation. Fifty-five soot blowers operated in the elevations of interest. Times of active soot blowing at any position in the elevation range of interest are represented in Fig. 6 by the semi-transparent vertical bands.

Overall, it may be observed from Fig. 6 that the heat flux substantially decreases with ascending boiler height, presumably due to heat siphoning from the flame into the steam tubes. When examining the narrow-angle radiometer data, the heat flux measurements overlap between replicates and fuel conditions. These data have much higher standard deviations than those of the ellipsoidal radiometer due to their narrow FOVs. This large variability shows the range of heat flux values from the different turbulent structures of the flame. The ellipsoidal radiometer collects rays from a much larger spatial area, averaging the highly luminous parts of the flame along with any cooler eddies together and, thus, has much smaller error bars. This difference in collection area also explains the consistently lower ellipsoidal radiometer averages when compared to the two NARs. Diffuse radiation was assumed to convert the NAR measured intensity to heat flux (Eq. (8)). All radiometers were directed toward the center of the radiant center of the boiler, but the ellipsoidal radiometer captured radiation from comparatively cooler areas on the periphery as well. This disparity between measurement techniques demonstrates that assuming diffuse reflection to convert the NAR intensity data to heat flux was not a completely valid assumption, despite the large size of the boiler. Even so, in general, the ellipsoidal data remain within the error bounds of the NARs.

Thus, generally, all three data sets overlap between fuel conditions (compare shaded areas at each floor level), implying the addition of biomass does not significantly change the heat flux profile of the boiler. The biomass measurement at Floor 10 shows a larger spread, but this is due to a single NAR measurement, which seems atypically high. If this measurement is considered an

Table 4 Average heat flux[a] as a function of boiler elevation and fuel blend

Floor	Blend heat flux (kW/m^2)	Coal heat flux (kW/m^2)	P-value
10	241.9 (219.0)	197.3	0.254 (0.545)
12	103.5	97.8	0.773
14	64.0	75.6	0.572

[a]Values in parentheses were calculated ignoring the single outlier taken by the CTH NAR during biomass co-firing.

outlier, the similarity between both fuel conditions increases. The variation between all measurements at a given condition and floor is presumably due to bias error between the different instruments (such as the averaging over different FOVs) and the timing of soot blowing and other transient changes in the furnace conditions. Costa et al. [34] measured heat flux at 39 points in the flame on two different runs. The average normalized difference between the two runs was 18%, despite extensive efforts to keep the operating conditions stable and avoid soot blowing. Encouragingly, the average normalized difference between the two UofU NAR replicates was quite similar at 15%.

The standard deviations of both NAR probes decrease with ascending height in the boiler. This decrease is presumably due to more flame uniformity with less turbulent fluctuations higher in the boiler, which matches visual observations made by the experimentalists at the time.

Care was taken to procure measurements during times with no active soot blowing; however, soot blowing did overlap with two of the UofU NAR measurements. These points are marked in Fig. 6 as solid black rectangles rather than the standard hollow markers, and these measurements occurred during replicates on Floors 10 and 12 during coal-only firing. In the case of Floor 10, when active soot blowing was noticed, the probe was removed, and a new data point was taken after the soot blowing was completed. For Floor 12, the probe remained in place before, during, and after the ~5 min soot blowing, as conditions proved hazardous to remove it.

Typically, one would expect to see flame heat flux increase with duration of time after soot blowing, since growing deposits inhibit heat absorption by the steam tubes. In this data set, this behavior is
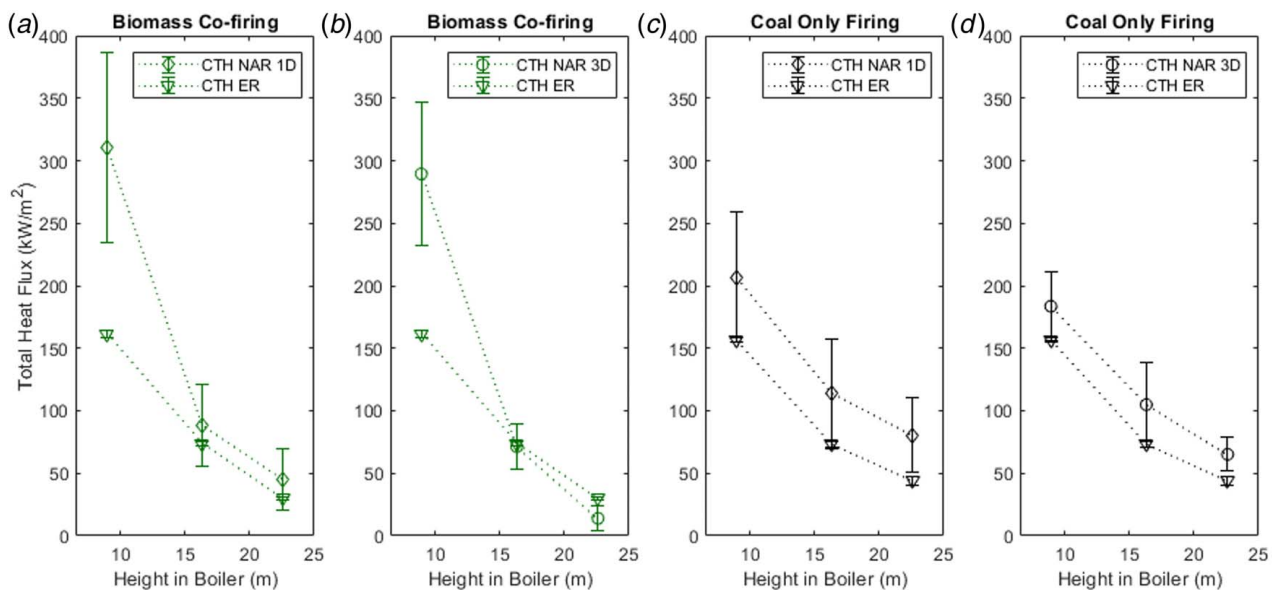

Fig. 7 Ellipsoidal radiometer total heat flux measurements compared to approximate, calculated heat flux from multiple NAR measurements presented as a function of floor (Plots b and d). Original single direction NAR heat flux measurements are presented for comparison (Plots a and c).

most clearly seen in the UofU NAR data during coal firing on Floor 12 (Fig. 6). However, this behavior is not as clearly seen in the case of coal firing on Floor 10, in which the first UofU replicate (first hollow rectangular data point) has a higher average heat flux than the second replicate (solid rectangular data point). However, during this second replicate, soot blowing began occurring somewhere in the boiler before producing a noticeable effect—which is when the replicate was aborted (note the vertical red line overlapping the second replicate before it was terminated in Fig. 6). This soot blowing may have affected the heat flux of the flame. It is also possible the heat flux profile of the boiler rhythmically shifts throughout the day due to soot blowing, ambient weather conditions (data were taken in August, so days were quite hot with cooler nights) and other unknown transient effects. Thus, perhaps there is not a constant heat flux value at a given boiler elevation but rather a range of typical values.

Table 4 summarizes the heat flux data at each boiler elevation and fuel condition averaged between the three radiometers. A student's t-test was performed on the data in order to ascertain the effect of replacing part of the coal with biomass. While there are only four data points per sample group, de Winter [42] concludes that t-tests can be safely applied for very small sample groups ($N \leq 5$) when the effects of the intervention are large. For this experiment, the null hypothesis was that the intervention of changing fuels did not change the heat flux profile of the boiler. P-values were calculated using the two-sample t-test and are presented in the final column of Table 4. P-values under a threshold value of 0.05 lead to a rejection of the null hypothesis, while values higher than 0.05 lead to the conclusion that the addition of biomass did not affect the heat flux profile to any large degree. The parenthetical values for Floor 10 were calculated without including the outlier replicate from the CTH NAR for that floor. Encouragingly, even when including the outlier at Floor 10, the lowest P-value is significantly larger than 0.05, which still leads to the conclusion that there is no significant change due to biomass co-firing. This result is promising for the implementation of co-firing regularly in the future.

Subplots B and D in Fig. 7 present the calculated total heat flux data from the CTH NAR probe (circular data points labeled "CTH NAR 3D"), which were calculated using the view factors presented in Table 3 and the measured radiative intensities at three different directions into the boiler. CTH NAR data at a single direction pointing into the center of the flame (triangular points labeled "NAR 1D") from Fig. 6 are presented again in this figure (subplots A and C) for ease of comparison along with the total heat flux measurements from the ellipsoidal radiometer ("CTH ER"). The green icons refer to the biomass co-firing case while the black icons refer to the coal-only case.

In similarity to the observations made in Fig. 6, apart from the calculated heat flux value at Floor 10 for the biomass co-firing case, the multi-directional NAR and the ellipsoidal radiometer data sets overlap fairly well, although the CTH NAR data are always higher in the coal-only case. When examining the difference between the single direction NAR measurements versus the multi-directional measurements, we see that for both fuel cases, the multi-directional measurements are closer to those of the ellipsoidal radiometer. This difference is due to the directional dependency of the flame radiation. It is predicted that increasing the number of measurement directions with the CTH NAR probe would decrease the difference seen between the two instruments.

5 Conclusions and Future Work

Heat flux data from three radiometers were taken at two different fuel cases (85% coal/15% torrefied, woody biomass co-firing versus firing only coal) and three different elevations in an industrial power plant. Intensity data from the two narrow-angle radiometers were converted to total heat flux assuming diffuse radiation in order to compare results between the three instruments. Multi-directional data from the Chalmers narrow-angle radiometer were also used to calculate a more accurate total heat flux to compare with the ellipsoidal radiometer data. Notable conclusions from the data are as follows:

- Heat flux substantially decreased with boiler height as heat was absorbed from the flame. Variation in heat flux over the collection time for a single data point also decreased with boiler height as the flame sheet became more uniform.
- The narrow-angle radiometers exhibited higher heat flux values and much larger standard deviations than the ellipsoidal radiometer data due to differences in each instrument's field of view. The narrow-angle instruments measured radiation from the hottest part of the flame and averaged radiation over a much smaller spatial area, resulting in higher radiation measurements and greater sensitivity to fluctuations in the flame.
- Calculated total heat flux values from the multi-directional Chalmers radiometer data were closer to the ellipsoidal results than the single direction measurements, although still overpredicted total heat flux. Adding more measurement directions presumably would increase that agreement even more. This disparity due to radiometer view angle indicates that the incident radiative intensity at the boiler ports is highly directional, despite the large size of the boiler. The effect of the cooler boiler periphery should be considered when analyzing and modeling radiative data in boilers.
- No obvious trends were observed in the heat flux measurements as a function of time since soot blowing, despite the fact that deposit growth inhibits heat transfer from the flame. This lack of pattern potentially indicates that the heat flux profile in the boiler is not constant and perhaps cycles periodically with time.
- Large variations between replicates at any given condition were observed. Presumably, this variation is due to a combination of factors, including instrument uncertainty, bias error between instruments, and changes in the nature of the flame as a function of time—one cause of which was certainly soot blowing. Despite this high variation in replicates, a student's t-test analysis on the data indicates that the biomass co-firing did not have any substantial effect on the heat flux profile as compared to coal-only firing.

Regarding future work of a similar nature taken in a similar setting, there are multiple improvements and ideas that could be implemented:

- *Increase the number of replicates at each floor and fuel condition.*
  Increasing the number of replicates would improve confidence in the statistical comparison between fuel conditions. In this campaign, the number of replicates was limited by duration of the fuel and the time it took to move equipment between floors. The use of multiple identical radiometers is recommended for future campaigns, as the equipment could be setup once and left in place. This approach would also provide the ability to take data at different elevations simultaneously, which would provide a better comparison between floors and a clearer temporal picture of the heat flux profile of the boiler.
- *Increase the number of narrow-angle radiometer measurements in various directions into the boiler.*
  This increase in directional measurements would enable a more direct comparison to any ellipsoidal radiometer results and would also yield valuable insight for modeling the boiler.
- *Increase repeatability in the operation of the radiometers.*
  This recommendation specifically applies to radiometer alignment in each port and the ambient temperature of the radiometers. Regarding alignment, custom rigs that allow for precise adjustments of the radiometer position and alignment is recommended. Ports must be kept closed except for short

windows of active measurement, so the ability to reinsert the radiometers precisely at the same position for every replicate would be ideal. This ability would require custom designs for each floor, as each port has different access constraints (see Fig. 1). Greater repeatability with instrument positioning could reduce differences between replicates, as the results showed that radiation from the cooler periphery can have a large impact on the measurements when changing radiometer direction. Regarding ambient temperature, thermopiles tend to be extremely sensitive to temperature gradients across the detector. The temperatures at the measurement locations were quite high ($\sim$55 °C). Cooling water jackets were used on all instruments while taking measurements, but with limited access to cooling water and the need to move between floors, the use of cooling jackets between measurements was intermittent. Ideally, all radiometers would remain in cooling jackets at all times to ensure a steady-state constant temperature profile across the radiometer thermopiles.

- *Increase replicates at a single location to gain better understanding of transient boiler effects.*

    It would be of great interest to systematically take replicates at a single port over a time period that included multiple soot blowing events. These replicates could provide insight into what the actual "steady-state" heat flux of the boiler is at a particular elevation. The data from this campaign imply that the heat flux at a given floor is not a constant value. Understanding the bounds of this variation would greatly aid in comparing different fuel conditions and in accurate modeling of the boiler.

In conclusion, the challenging nature of taking data in an industrial setting and the associated constraints make it difficult to procure copious data sets. However, it appears the heat flux profile between biomass co-firing and coal-only firing is unchanged—or at least that the change is below the level of measurement resolution. These results bode well for the ability of the plant to implement biomass co-firing at the levels investigated as a reasonable option to utilize biomass from forest management and to reduce net greenhouse gas emissions.

Conflict of Interest

There are no conflicts of interest. This article does not include research in which human participants were involved. Informed consent not applicable. This article does not include any research in which animal participants were involved.

Data Availability Statement

The datasets generated and supporting the findings of this article are obtainable from the corresponding author upon reasonable request.

Nomenclature

A = area (m^2)
E = total radiative heat flux (kW/m^2)
F = view factor
I = radiative intensity (kW/m^2/sr)
T = temperature (K)
V = voltage (mV)
$\Re$ = electrical responsivity (mV/kW)
K_1 = instrument model parameter 1 (kW/m^2/mV/sr)
K_2 = instrument model parameter 2 (kW/m^2/K^4/sr)
K_3 = instrument model parameter 3 (kW/m^2/K^4/sr)
K_4 = instrument model parameter 4 (K/mV)
R_t = thermal resistance (K/kW)

Greek Symbols

θ = polar angle from probe tip to surface (rad)
ϕ = solid angle from narrow wall sections to probe tip
Φ = radiative power (kW)
Ω = solid angle from surface to probe tip

Superscripts and Subscripts

a = ambient environment of radiometer thermopile
d = thermopile detector
e = emitted
i = view factor radiating surface
j = view factor intercepting surface
s = radiation source
w = radiometer view tube walls
B = view factor surface, bottom of boiler
E = electrical output of power plant
L = view factor surface, left wall of boiler
O = view factor surface, opposite wall of boiler
R = view factor surface, right wall of boiler
T = view factor surface, top of boiler
SH = view factor surface, superheater section of boiler

References

[1] Biomass Explained, 2022, U. S. Energy Information Administration (EIA), https://www.eia.gov/energyexplained/biomass/, Accessed March 21, 2022.

[2] Dreizler, A., Pitsch, H., Scherer, V., Schulz, C., and Janicka, J., 2021, "The Role of Combustion Science and Technology in Low and Zero Impact Energy Transformation Processes," Appl. Energy Combust. Sci., 7.

[3] Goerndt, M. E., Aguilar, F. X., Miles, P., Shifley, S., Song, N., and Stelzer, H., 2012, "Regional Assessment of Woody Biomass Physical Availability as an Energy Feedstock for Combined Combustion in the US Northern Region," J. Forestry, 110(3), pp. 138–148.

[4] Xu, Y., Yang, K., Zhou, J., and Zhao, G., 2020, "Coal-Biomass Co-Firing Power Generation Technology: Current Status, Challenges and Policy Implications," Sustainability, 12(9), p. 3692.

[5] Langholtz, M. H., Stokes, B. J., and Eaton, L. M., 2016, Billion-Ton Report: Advancing Domestic Resources for a Thriving Bioeconomy, Volume 1: Economic Availability of Feedstock. Technical Report, U. S. Department of Energy, Oak Ridge National Laboratory, Oak Ridge, TN. ORNL/TM-2016/160, p. 448.

[6] Karampinis, E., Grammelis, P., Agraniotis, M., Violidakis, I., and Kakaras, E., 2014, "Co-Firing of Biomass With Coal in Thermal Power Plants: Technology Schemes, Impacts, and Future Perspectives," Wiley Interdiscip. Rev.: Energy Environ., 3, pp. 384–399.

[7] Sami, M., Annamalai, K., and Wooldridge, M., 2001, "Co-Firing of Coal and Biomass Fuel Blends," Prog. Energy Combust. Sci., 27(2), pp. 171–214.

[8] Hughes, E. E., and Tillman, D. A., 1998, "Biomass Cofiring: Status and Prospects," Fuel Process. Technol., 54(1–3), pp. 127–142.

[9] Tillman, D. A., 2000, "Biomass Cofiring: The Technology, the Experience, the Combustion Consequences," Biomass Bioenergy, 19(6), pp. 365–384.

[10] Steer, J., Marsh, R., Griffiths, A., Malmgren, A., and Riley, G., 2013, "Biomass Co-Firing Trials on a Down-Fired Utility Boiler," Energy Convers. Manage., 66, pp. 285–294.

[11] Zuwala, J., and Sciazko, M., 2010, "Full-Scale Co-Firing Trial Tests of Sawdust and Bio-Waste in Pulverized Coal-Fired 230t/h Steam Boiler," Biomass Bioenergy, 34(8), pp. 1165–1174.

[12] Eddings, E. G., McAvoy, D., and Coates, R. L., 2017, "Co-Firing of Pulverized Coal With Pinion Pine/Juniper Wood in Raw, Torrefied and Pyrolyzed Forms," Fuel Process. Technol., **161**, pp. 273–282.

[13] Fakourian, S., Li, X., Wang, Y., Wendt, J. O., and Fry, A., 2022, "Ash Aerosol and Deposit Formation From Combustion of Coal and Its Blend With Woody Biomass at Two Combustion Scales: Part 1–1.5 MW$_{TH}$ Pilot-Scale Combustor Tests," Energy Fuels, **36**(1), pp. 554–564.

[14] Holtmeyer, M. L., Li, G., Kumfer, B. M., Li, S., and Axelbaum, R. L., 2013, "The Impact of Biomass Cofiring on Volatile Flame Length," Energy Fuels, **27**(12), pp. 7762–7771.

[15] Li, J., Brzdekiewicz, A., Yang, W., and Blasiak, W., 2012, "Co-Firing Based on Biomass Torrefaction in a Pulverized Coal Boiler With Aim of 100% Fuel Switching," Appl. Energy, **99**, pp. 344–354.

[16] Lu, G., Yan, Y., Cornwell, S., Whitehouse, M., and Riley, G., 2008, "Impact of Co-Firing Coal and Biomass on Flame Characteristics and Stability," Fuel, **87**(6), pp. 1133–1140.

[17] Luan, C., You, C., and Zhang, D., 2014, "Composition and Sintering Characteristics of Ashes From Co-Firing of Coal and Biomass in a Laboratory-Scale Drop Tube Furnace," Energy, **69**(5), pp. 562–570.

[18] Moon, C., Sung, Y., Ahn, S., Kim, T., Choi, G., and Kim, D., 2013, "Effect of Blending Ratio on Combustion Performance in Blends of Biomass and Coals of Different Ranks," Exp. Therm. Fluid. Sci., **47**(5), pp. 232–240.

[19] Alobaid, F., Busch, J., Stroh, A., Ströhle, J., and Epple, B., 2020, "Experimental Measurements for Torrefied Biomass Co-Combustion in a 1 MW$_{th}$ Pulverized Coal-Fired Furnace," J. Energy Inst., **93**(6), pp. 833–846.

[20] Li, H., Chi, H., Han, H., Hu, S., Song, G., Wang, Y., He, L., Wang, Y., Su, S., and Xiang, J., 2021, "Comprehensive Study on Co-Combustion Behavior of Pelletized Coal-Biomass Mixtures in a Concentrating Photothermal Reactor," Fuel Process. Technol., **211**(1), p. 106596.

[21] Bäckström, D., Johansson, R., Andersson, K., Wiinikka, H., and Fredriksson, C., 2015, "On the Use of Alternative Fuels in Rotary Kiln Burners—An Experimental and Modelling Study of the Effect on the Radiative Heat Transfer Conditions," Fuel Process. Technol., **138**(7), pp. 210–220.

[22] Milićević, A., Belošević, S., Crnomarković, N., Tomanović, I., Stojanović, A., Tucaković, D., Deng, L., and Che, D., 2021, "Numerical Study of Co-Firing Lignite and Agricultural Biomass in Utility Boiler Under Variable Operation Conditions," Int. J. Heat. Mass. Transfer., **181**(12), p. 121728.

[23] Qin, L., Lu, G., Hossain, M. M., Morris, A., and Yan, Y., 2022, "A Flame Imaging-Based Online Deep Learning Model for Predicting NO$_X$ Emissions From an Oxy-Biomass Combustion Process," IEEE Trans. Instrum. Meas., **71**, pp. 1–11.

[24] Fry, A., Adams, B., Paschedag, A., Kazalski, P., Carney, C., Oryshchyn, D., Woodside, R., Gerdemann, S., and Ochs, T., 2011, "Principles for Retrofitting Coal Burners for Oxy-Combustion," Int. J. Greenhouse Gas Control, **5S**, pp. S151–S158.

[25] Bäckström, D., Johansson, R., Andersson, K., Johnsson, F., Clausen, S., and Fateev, A., 2014, "Measurement and Modeling of Particle Radiation in Coal Flames," Energy Fuels, **28**(3), pp. 2199–2210.

[26] Andersson, K., Johansson, R., Hjärtstam, S., Johnsson, F., and Leckner, B., 2008, "Radiation Intensity of Lignite-Fired Oxy-Fuel Flames," Exp. Therm. Fluid. Sci., **33**(10), pp. 67–76.

[27] Andersson, K., Johansson, R., Johnsson, F., and Leckner, B., 2008, "Radiation Intensity of Propane-Fired Oxy-Fuel Flames: Implications for Soot Formation," Energy Fuels, **22**(5), pp. 1535–1541.

[28] Bäckström, D., Gall, D., Pushp, M., Johansson, R., Andersson, K., and Pettersson, J. B., 2015, "Particle Composition and Size Distribution in Coal Flames – The Influence on Radiative Heat Transfer," Exp. Therm. Fluid. Sci., **64**(6), pp. 70–80.

[29] Burchfield, N. A., 2020, "Narrow Angle Radiometer For Oxy-Coal Combustion," Master's thesis, https://scholarsarchive.byu.edu/etd/8423/

[30] Dobó, Z., Backman, M., and Whitty, K. J., 2019, "Experimental Study and Demonstration of Pilot-Scale Oxy-Coal Combustion at Elevated Temperatures and Pressures," Appl. Energy, **252**(10), p. 113450.

[31] Fry, A., Spinti, J., Preciado, I., Diaz-Ibarra, O., and Eddings, E., 2015, "Pilot-Scale Investigation of Heat Flux and Radiation From an Oxy-Coal Flame," 40th International Technical Conference on Clean Coal and Fuel Systems, Clearwater, FL, May 31–June 4.

[32] Gunnarsson, A., Bäckström, D., Johansson, R., Fredriksson, C., and Andersson, K., 2017, "Radiative Heat Transfer Conditions in a Rotary Kiln Test Furnace Using Coal, Biomass, and Cofiring Burners," Energy Fuels, **31**(7), pp. 7482–7492.

[33] Viskanta, R., and Mengüc, M. P., 1987, "Radiation Heat Transfer in Combustion Systems," Prog. Energy Combust. Sci., **13**, pp. 97–160.

[34] Costa, M., Azevedo, J. L., and Carvalho, M. G., 1997, "Combustion Characteristics of a Front-Wall-Fired Pulverized-Coal 300 MW$_E$ Utility Boiler," Combust. Sci. Technol., **129**, pp. 277–293.

[35] Li, Z., Jing, J., Liu, G., Chen, Z., and Liu, C., 2010, "Measurement of Gas Species, Temperatures, Char Burnout, and Wall Heat Fluxes in a 200-MW$_E$ Lignite-Fired Boiler at Different Loads," Appl. Energy, **87**, pp. 1217–1230.

[36] Butler, B. W., and Webb, B. W., 1991, "Local Temperature and Wall Radiant Heat Flux Measurements in an Industrial Scale Coal Fired Boiler," Fuel, **70**, pp. 1457–1464.

[37] Butler, B. W., and Webb, B. W., 1993, "Measurement of Radiant Heat Flux and Local Particle and Gas Temperatures in a Pulverized Coal-Fired Utility-Scale Boiler," Energy Fuels, **7**, pp. 835–841.

[38] Li, X., Fakourian, S., Moyer, B., Wendt, J. O. L., and Fry, A., 2022, "Ash Aerosol and Deposit Formation From Combustion of Coal and Its Blend With Woody Biomass at Two Combustion Scales: Part 2—Tests on a 471 MW$_E$ Full-Scale Boiler," Energy Fuels, **36**, pp. 565–574.

[39] Allgurén, T., Andersson, K., Fry, A., and Eddings, E. G., 2022, "NO Formation During Co-Combustion of Coal With Two Thermally Treated Biomasses," Fuel Process. Technol., **235**, p. 107365.

[40] Dobó, Z., 2018, "Heat Radiation Measurement Method for High Pressure Oxy-Fuel Combustion," Measurement, **124**, pp. 191–196.

[41] Spinti, J. P., Smith, S. T., Smith, P. J., Harding, N. S., Scheib, K., and Draper, T. S., 2021, "Using Bayesian Analysis to Quantify Uncertainty in Radiometer Measurements," J. Verif. Valid. Uncertain. Quantifi, **6**(1), p. 011003.

[42] de Winter, J. C. F., 2013, "Using the Student's t-test With Extremely Small Sample Sizes," Pract. Assess. Res. Eval., **18**(10), pp. 1–12.